Ultrafast Energy Transfer in LHC-II Revealed by Three-Pulse Photon Echo Peak Shift Measurements

Ritesh Agarwal,[†] Brent P. Krueger,[†] Gregory D. Scholes,[†] Mino Yang,[†] Jenny Yom,[†] Laurens Mets,[‡] and Graham R. Fleming*,[†]

Department of Chemistry, University of California, Berkeley, and Physical Biosciences Division, Lawrence Berkeley National Laboratory, Berkeley, California 94720-1460, and Department of Molecular Genetics and Cell Biology, The University of Chicago, 1101 E. 57th Street, Chicago, Illinois 60637

Received: May 11, 1999; In Final Form: January 21, 2000

We report the results of three-pulse photon echo peak shift (3PEPS) measurements on the light-harvesting complex II (LHC-II) of the green algae *Chlamydomonas reinhardtii*. Experiments were performed at two different excitation wavelengths, 670 and 650 nm, corresponding to Chl-*a* and Chl-*b* excitation, respectively. The 3PEPS data are analyzed using a new theory that incorporates the effect of energy transfer on third-order response functions. Our theoretical model separates energy transfer dynamics from the solvation dynamics arising from coupling of the electronic transitions to the protein environment. We suggest that the protein fluctuations can be described by an ultrafast solvation on a sub-100 fs time scale and a long time correlation (static disorder). Decay of the 670 nm peak shift reveals spectral equilibration time scales for Chl-*a* molecules that range from 300 fs to 6 ps and agree well with other experiments. 3PEPS data at 650 nm (Chl-*b* excitation) reveal rapid Chl-*b* to Chl-*b* energy transfer (<1 ps), which suggests excitation hopping between a pair of Chls-*b*, and slow energy transfer from these Chls-*b* to Chls-*a*. Also, a 60 cm^{-1} oscillatory mode is observed for Chl-*b* which we attribute to the first observation of coherent nuclear dynamics in LHC-II. Calculating the energy transfer dynamics based on recently proposed assignments of chromophores by solving the master equation reveals Chl-*b* intra- and interband energy transfer dynamics that are in qualitative agreement with the simulation model of the peak shift data.

1. Introduction

The initial steps of photosynthesis are accomplished with remarkable efficiency. They involve the capture of sunlight (light harvesting) by the pigment−protein antenna complexes, followed by transfer of this energy to the reaction centers. There, a series of fast, vectorial electron transfer reactions generate a membrane potential and, in turn, a pH gradient across the membrane.[1−7]

The antenna complexes of photosynthetic organisms play a central role in optimizing the efficacy of the conversion of incident radiation to usable energy. The arrangement of several antenna complexes, each consisting of a dozen or more pigments in close mutual proximity, in connection with a single reaction center is typical, thereby providing a high spatial and spectral absorption cross section for the associated reaction center. Approximately half the chlorophyll present in the chloroplasts of green plants and green algae is bound in LHC-II.[8] This complex absorbs light and transfers energy with high efficiency to the photosystem II reaction center. According to the 3.4 Å resolution atomic model of Kühlbrandt et al.,[9] LHC-II contains two carotenoid, seven Chl-*a* (chlorophyll-*a*), and five Chl-*b* molecules. Biochemical assays suggest that at least one carotenoid and one or two chlorophylls are missing from the crystal structure.[4,10] Neither the exact orientation nor the identities of Chl-*a* and Chl-*b* cofactors are resolved in the crystal structure. Assignments of these chlorophylls must still be determined before detailed structure−function studies, such as those reported for bacterial antenna complexes,[2,3,11−13] can be undertaken for LHC-II.

In light of their inability to differentiate between Chl-*a* and Chl-*b* in the structural data, Kühlbrandt et al.[9] made the reasonable assumption that Chls-*b* and Chls-*a* must be close together to facilitate rapid Chl-*b* to Chl-*a* energy transfer (EET). Furthermore, they supposed that the lower energy Chl-*a* pigments (where excitation energy persists for long times) must be closest to the carotenoids, which protect the complex by quenching excited triplet states. These assumptions led to the assignment wherein the seven Chls-*a* are in close proximity to the central luteins and the five Chls-*b* are located on the periphery of the complex.

Recent modeling of time-resolved and polarized absorption data, as well as comparison to the almost-homologous core antenna CP29, has led to tentative assignments of orientations of the chlorophyll transition moments.[14−16] It was suggested that, although the current body of data is reasonably consistent with the Kühlbrandt assignments, interchanging the positions of one or two Chls-*b* and Chls-*a* may provide a better structural basis for modeling the data.[14−16] Recently, Kuhlbrandt and co-workers[17] have reported a site directed mutation study of LHC-II complexes in which they knock out specific chlorophyll binding sites. They confirmed that Chls-*a1*, *-a2*, *-a3*, and *-b5*, *-b6* are indeed Chls-*a* or *-b* respectively and suggested that Chl-*b3* is actually Chl-*a*. Their results suggest incomplete specificity in some of these sites. Using similar methodology, Bassi et al.[18] have analyzed the highly homologous CP29 protein and reported that four porphyrin-binding sites (Chls-*a1*, *-a2*,

[†] University of California and Lawrence Berkeley National Laboratory.
[‡] The University of Chicago.

10.1021/jp9915578 CCC: $19.00 © 2000 American Chemical Society
Published on Web 03/11/2000

-a4, and *-a5*) are selective for Chls-*a*, whereas four other sites (Chls-*a3*, *-b3*, *-b5*, and *-b6*) have mixed Chl-*a*/Chl-*b* specificity. This implies that these complexes could have either a Chl-*a* or Chl-*b* at some sites.

The steady state absorption spectrum of LHC-II at room temperature has a maximum centered around 676 nm attributed to the Q_y transition of Chl-*a* pigments, and a shoulder around 650 nm assigned to Chl-*b* transitions. The structure of the Q_y band of LHC-II at low temperatures was investigated with linear and circular dichroism spectroscopy, which revealed at least six or possibly nine chlorophyll transitions.[19] Further spectroscopic characterization of LHC-II trimers revealed that the Chl-*b* region is composed of at least five bands near 640, 647, 649, 652, and 656 nm.[20] The Chl-*a* absorption was found to be composed of subbands near 661, 668, 671, 673, and 676 nm. These results also suggested the existence of possible excitonic coupling between the pigments.[19,20] It is not known if the subbands observed in the CD spectra of LHC-II correspond to individual Chl site absorption or to delocalized excitations shared between the Chls (excitonic interactions).

The current body of time-resolved data has been useful for the identification of Chl-*b* to Chl-*a* and Chl-*a* to Chl-*a* energy transfer with time scales ranging from ~150 fs to ~10 ps.[21−29] The mechanism of energy migration is determined by an interplay between disorder, homogeneous broadening dynamics and electronic factors. Thus, in order to understand in detail the dynamics of energy transfer within a multichromophoric antenna, one needs information on the electronic coupling between molecules,[30,31] the site-to-site disorder of the zero-order excitation energies (and perhaps of the couplings),[32,33] the coupling to the protein (i.e., electron−phonon coupling),[34] and the time scales of protein relaxation and of energy transfer. All except the electronic couplings can be obtained from femtosecond nonlinear spectroscopy.[35,36]

Three-pulse photon echo peak shift (3PEPS) data obtained for excitation wavelengths resonant with the Chl-*a* (670 nm) and Chl-*b* (650 nm) absorption bands of trimeric LHC-II are reported in the present work. The utility of 3PEPS measurements for probing the details of ultrafast energy transfer (described in section 3) in purple bacterial LHCs has been demonstrated recently.[37−39] To apply the 3PEPS technique to a system as complex as LHC-II requires extension of the theory[40] and a clear distinction between energy transfer that maintains the excitation within the laser spectrum ("intraband") or removes it from that spectral region ("interband"). For the LHC-II system, the experiment is designed such that energy transfer between either the Chls-*a* or Chls-*b* molecules corresponds to intraband energy transfer, while energy transfer from Chl-*b* to Chl-*a* corresponds to interband energy transfer. Identification of energy transfer between Chl-*b* pigments or between similar spectral types of Chl-*a* (which we refer to as intraband if it occurs within our laser pulse spectrum) is difficult using standard time-resolved methods such as transient absorption or time-resolved fluorescence. In contrast, the 3PEPS technique is primarily sensitive to intraband energy transfer processes as illustrated recently by Yang and Fleming who elucidated the effect of energy transfer on the nonlinear response functions.[40] The effect of interband energy transfer on the peak shift—that is, when the excitation energy moves out of the laser window—is more subtle, but must also be considered in the present work to account for Chl-*b* to Chl-*a* energy transfer. In this respect, transient grating spectroscopy provides a complementary tool because it is sensitive to population dynamics; therefore, energy migration to a "dark state", i.e., a state which does not absorb within the bandwidth of the pulse, should show up as a decay contribution to the signal.

In this paper we focus on elucidating the dynamics of energy redistribution within the Chl-*b* absorption band prior to energy transfer to the Chl-*a* pigments. We identify evidence for rapid energy hopping between a Chl-*b* pair and relate this to dynamic models for the antenna. We also discuss this observation in the context of Chl-*a* band energy redistribution.

2. Experimental Section

Thylakoid membranes were prepared from the *Chlamydomonas reinhardtii* PS I-PSII double-deficiency strain C2. The C2 strain contains peripheral antenna LHC proteins, but lacks both the chloroplast Ps*b*A gene and the chloroplast tscA gene.[41] Thus, the strain is missing all of the proteins of the PSI and PSII reaction centers and core antenna.[42,43] The strain retains the peripheral antenna LHC proteins, primarily LHC-II, but possibly including LHC-I as well.[41−43] LHC-containing thylakoids were isolated and suspended in a sorbitol buffer for 1 min and then microcentrifuged (8000 rpm, 10 min). These samples were stored at −70 °C. In order to minimize scattering, each thawed LHC-II sample was sonicated and centrifuged immediately prior to measurement. The sample was flowed through a 200 μm path length cell using a peristaltic pump (ca. 2.5 mL sample reservoir; chilled with recirculating water bath at 4 °C).

The experiments were performed using a mode-locked Ti:sapphire laser (Coherent Mira seed) pumped with a Coherent INNOVA 425 Ar^+ laser. The resulting pulses, centered at 800 nm at a repetition rate of ~76 MHz, were then stretched by a grating expander before being amplified by a regenerative amplifier (Coherent RegA 9050). The amplified pulses were compressed and fed to an optical parametric amplifier (Coherent OPA 9450) to generate pulses centered at 650 and 670 nm with a fwhm of 40 fs and a repetition rate of 250 kHz. The average pulse energy at the sample was approximately 4 nJ per pulse, per beam. Experiments using lower pulse energies (50%) did not reveal any unusual power dependence of the data.

The three-pulse photon echo peak shift and transient grating measurements were carried out as previously described.[44] In short, three laser beams (parallel-polarized) are arranged in an equilateral triangle geometry and focused into the sample. The first pulse interacts with the sample to create an optical coherence, the second pulse creates a population, in either the ground or excited state, and the third pulse creates a second coherence. If the phase of the second coherence period is opposite to that of the first, an echo signal is produced. The time-integrated echo profiles are simultaneously measured in two phase-matched directions, $\mathbf{k} = \mathbf{k}_3 \pm (\mathbf{k}_1 - \mathbf{k}_2)$, as a function of coherence period. The echo peak shifts obtained from the echo profiles are recorded as a function of population period. If the first two pulses are temporally overlapped, the pulse creates a spatial population grating. In the transient grating measurements, the third pulse is diffracted from such grating, and the intensity of the diffracted pulse in the $\mathbf{k} = \mathbf{k}_3 \pm (\mathbf{k}_1 - \mathbf{k}_2)$ direction is measured as a function of the delay time. The grating is destroyed by population decay, that is, transient grating gives the excited state lifetime.

3. Simulation Model for the 3PEPS Data

The electronic energy gaps of chromophores in the condensed phase can be described as a two-level system with a fluctuating optical transition frequency $\omega_{eg}^{i}(t)$ of the *i*th chromophore. These fluctuations can be modeled as

$$\omega_{eg}^{i}(t) = \langle\omega_{eg}\rangle + \delta\omega_{eg}(t) + \Delta_i \quad (1)$$

where $\langle\omega_{eg}\rangle$ is the average transition frequency between ground, g, and excited, e, states and Δ_i is the static (slow) offset from the mean which depends on the local environment of that chromophore. $\delta\omega_{eg}(t)$ denotes the dynamic (fast) contributions to the transition frequency and is characterized by the correlation function of eq 2

$$M(t) = \frac{\langle\delta\omega_{eg}(0)\ \delta\omega_{eg}(t)\rangle}{\langle\delta\omega_{eg}^{2}\rangle} \quad (2)$$

$M(t)$ is often modeled as a sum of a Gaussian, exponentials, and damped cosines, as in eq 3[45]

$$M(t) = (\langle\Delta\omega_g^2\rangle e^{-(t/\tau_g)^2} + \sum_n \langle\Delta\omega_n^2\rangle e^{-t/\tau_n} + \sum_j \langle\Delta\omega_j^2\rangle e^{-t/\tau_j}\cos(\omega_j t + \phi_j))/\sum_k \langle\Delta\omega_k^2\rangle + \Delta_{in}^{\ 2} \quad (3)$$

where $\langle\Delta\omega^2\rangle$ is the coupling strength for each term, τ_k are time constants, ω_j are the frequencies of coherently excited vibrations, and ϕ_j are the corresponding phase factors, and Δ_{in} is the inhomogeneous width, i.e., the standard deviation of the distribution of Δ_i values (from eq 1). The index, k, in the denominator includes all g, n, and j. The line-broadening function, $g(t)$, which characterizes the spectral distribution of the fluctuations, is calculated from M(t) and is used to calculate the nonlinear optical response functions.[46]

In an aggregate system, where there are interactions *between* chromophores, interchromophore energy transfer modifies the nonlinear response functions.[37] Recently, Yang and Fleming have developed a theory for multichromophoric systems coupled to a harmonic bath.[40] This theory is formally exact for weak coupling between the chromophores. The system is modeled as a collection of dimers (donor and acceptor associated with the *intraband* energy transfer) that can each also undergo interband energy transfer processes. The fluctuations induced by the bath are assumed to be completely uncorrelated in the donor and acceptor. Third-order response functions are obtained by the three interactions of the dimer with the electric fields of the excitation pulses. Energy transfer within (intraband) and outside (interband) the laser spectrum is incorporated by introducing new pathways that contribute to the third order nonlinear polarization. A simplified picture (shown in Figure 1), in terms of double-sided Feynman diagrams, gives an intuitive understanding of the peak shift for an intraband energy transfer system coupled to interband energy transfer processes. The first term (describing the dynamics of the density matrix exciton−hole pair on the donor) arises when the three pulses interact only with the donor; i.e., there is no contribution from energy transfer dynamics. This pathway has rephasing capability and hence can produce an echo signal. The second term describes the dynamics of the density matrix exciton−hole pair after it has migrated to the acceptor: it comes from the third-order process due to interaction of the first two pulses with the donor and the third with the acceptor. This pathway has no rephasing capability for uncorrelated baths and hence gives a free induction decay (FID) signal. The total third-order nonlinear polarization is given by the sum of the two terms. The peak shift, measuring the rephasing capability of the nonlinear polarization, decreases as the relative contribution of the FID to the echo signal increases. $P_D(T)$ and $P_A(T)$ are the probabilities of finding the exciton on the donor and acceptor

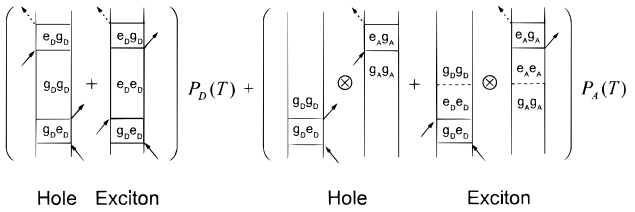

Figure 1. A simplified picture of the model used to simulate the peak shift in the case of intra- and interband energy transfer. Feynman diagrams are shown for self-polarization (first diagram) and cross polarization (second diagram) terms.[40] The arrows indicate the interaction of the dimer with the incoming fields. The terms g,e stand for ground, and excited state, respectively, while D,A stand for donor and acceptor. For more details, refer to section 3 of the text.

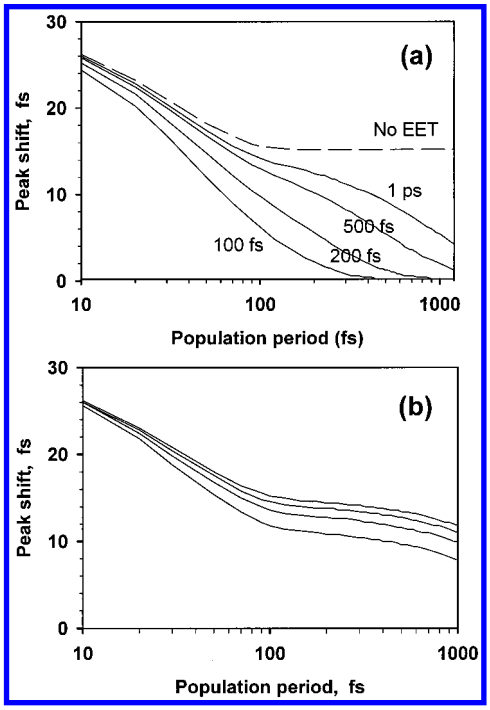

Figure 2. (a) Illustrative calculations of peak shifts vs population periods for different intraband energy transfer rates for a model system. The intraband transfer rates are given with each curve. The $M(t)$ consists of a Gaussian decay and an inhomogeneous term. The peak shift decays rapidly with increasing intraband energy transfer rates. Note the logarithmic scale for population period times. (b) Illustrative peak shift calculations for different interband transfer rates with the intra band transfer rate fixed at 4 ps in all cases. The interband transfer rates are 100, 200, 500, and 20 000 fs from bottom to top. Clearly evident is the fact that the peak shift does not decay to zero with fast interband transfer rates. Note the logarithmic scale for population period times.

molecules, which control the relative contribution of echo and FID signals, respectively. These probabilities can decay owing to interband energy transfer occurring on each site and also can be transferred from donor to acceptor by intraband energy transfer. As a result, the intra- and interband energy transfer rates affect the peak shift behavior by controlling the relative intensities of the echo and FID signals. We emphasize that the FID signal resulting in decay of the peak shift is only generated by the *intraband* energy transfer process, though the interband energy transfer controls the population of the donor and acceptor associated with intraband energy transfer and, thus, does affect the peak shift indirectly.

Model calculations in the absence of interband energy transfer are shown in Figure 2a using an $M(t)$ that consists of a Gaussian component and finite inhomogeneity ($M(t) = \langle\Delta\omega_g^2\rangle e^{-(t/\tau_g)^2} + \Delta_{in}^{\ 2}$, where $\langle\Delta\omega^2\rangle^{1/2} = 120\ cm^{-1}$, $\tau_g = 70$ fs, and $\Delta_{in} = 200$

cm^{-1}) to describe the bath dynamics. Intraband energy transfer rates are varied from $(100\ fs)^{-1}$ to $(1\ ps)^{-1}$, and the peak shift decay reflects these time scales.

For the case of intraband energy transfer, an approximate relationship was derived in ref 40

$$\tau^*(T) = \tau_0^*(T)\exp(-k_{EET}T) \quad (4)$$

where $\tau_0^*(T)$ is the peak shift in the absence of energy transfer, i.e., for noninteracting chromophores. This peak shift, $\tau_0^*(T)$, results from the solvation dynamics of the excited chromophores owing to their interaction with the protein environment (e.g., the simple $M(t)$ given above). This equation shows that, for energy transfer to a chromophore absorbing within the laser bandwidth, solvation dynamics can be separated from energy transfer dynamics. Numerical simulations confirmed the validity of eq 4 for a homogeneous distribution of energy transfer rates (i.e., single energy transfer rate).[40]

The interband energy transfer process (energy transfer out of the laser spectrum window) has a more subtle effect on the peak shift.[40] As a consequence of migration of the density matrix exciton−hole pair out of the laser window, the pair cannot interact with the third pulse, thus no FID (or echo) signal is generated, and the grating intensity that generates an echo signal decreases. In this case of *only* interband energy transfer, the rephasing capability of the system does not change, nor does the peak shift. Model calculations are shown in Figure 2b for the above-mentioned $M(t)$, a fixed (slow) intraband transfer rate of $(4\ ps)^{-1}$, and various interband transfer rates, which are the same for both the donor and acceptor. Figure 2b clearly shows that the peak shift does not decay to zero (as it did for the case of intraband energy transfer) when there is only an interband energy transfer process (or very slow intraband energy transfer as in this case). The slightly faster decay for the case of fast interband transfer is due to energy transfer processes occurring within the duration of the laser pulse. This effect is relatively minor compared to that arising from generation of FID in the intraband energy transfer case.

In a system which undergoes both (fast) intra- and interband energy transfer, the situation is more complex. For example, consider a simplified system

$$a \xleftarrow{k_{inter}} b_5 \xrightarrow{k_{intra}} b_6 \xrightarrow{k'_{inter}} a \quad (5)$$

where a and b represent Chl-*a* and Chl-*b*, respectively. When b_5 is initially excited, the Chl-*b* population kinetics are given by

$$[b_5] = [b_5]_0 e^{-(k_{inter}+k_{intra})T}$$

$$[b_6] = [b_5]_0 \frac{k_{intra}}{k_{intra} + k_{inter} - k'_{inter}}[e^{-k'_{inter}T} - e^{-(k_{inter}+k_{intra})T}] \quad (6)$$

where $[b_5]_0$ is the initial population of b_5, and $[b_5]$ and $[b_6]$ are the populations of b_5 and b_6 at time T. Decay of the peak shift associated with intraband energy transfer arises from the *relative* amplitude of the FID (proportional to $[b_6]$) to the echo signal (proportional to $[b_5]$), which increases as the intraband energy transfer proceeds. When $k_{inter} = k'_{inter}$, we obtain $[b6]/[b5] = (1 - \exp(-k_{intra}T)/\exp(-k_{intra}T)$, which suggests that the peak shift is insensitive to the interband energy transfer. When $k_{inter} \neq k'_{inter}$, the ratio $[b_6]/[b_5]$ has a dependence on the interband energy transfer rates as does the peak shift. The simple illustration of these two cases shows that interband energy transfer *combined with* intraband energy transfer appears in the peak shift in a complicated way; the time scales of the peak shift decay associated with energy transfer may not have any direct correspondence to either the population kinetics or to any pairwise transfer rate, and must be calculated from a kinetic model and the appropriate response functions.

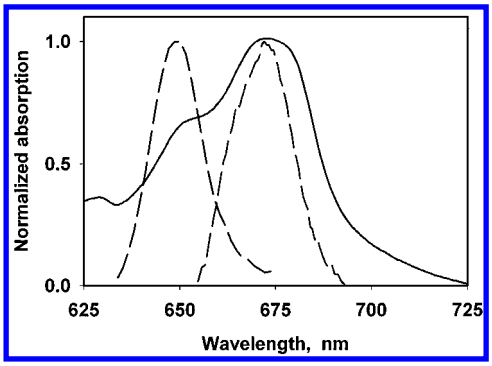

Figure 3. Absorption spectrum of LHC-II at room temperature (solid line) along with the spectra of the laser pulses (dashed lines) centered at 670 and 650 nm.

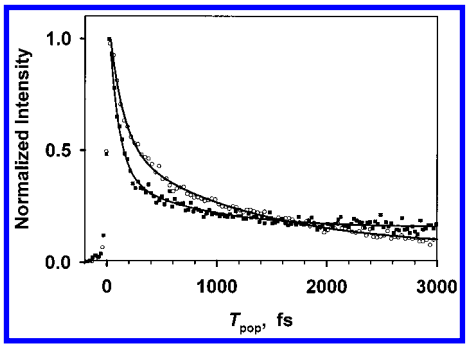

Figure 4. Transient grating data for LHC-II. Filled squares are for Chl-*b* (650 nm) excitation, open circles for Chl-*a* (670 nm) excitation. The solid lines through the data points are double-exponential fits to the transient grating data. See section 4A for fit parameters.

The theory developed by Yang and Fleming can also incorporate multiexponential energy transfer rates.[40] In the present paper, we use their approach to analyze the 3PEPS data. In all the simulations we take into account the finite duration of the laser pulses, and use exact expressions for the peak shift (rather than the approximate expressions given here for clarity).

4. Results and Discussion

Transient grating and three-pulse echo experiments were performed on LHC-II at two different excitation wavelengths: 670 and 650 nm, which correspond to absorption maxima of Chl-*a* and Chl-*b*, respectively. The absorption spectrum of this LHC-II preparation is given in Figure 3 along with the laser pulse spectra for both the excitation wavelengths.

4A. Transient Grating. In transient grating measurements, the first two pulses interact with the sample simultaneously, creating a spatial population grating. The third pulse, which undergoes a Bragg diffraction from this grating, measures the lifetime of the grating. The induced grating is destroyed by population decay; hence the transient grating data contains information primarily about interband energy transfer dynamics.

The transient grating signal at 670 nm is found to decay biexponentially with time constants of 160 fs (∼60%) and 2ps (∼30%) along with a ∼10% nondecaying (or very slow) component as shown (open circles) in Figure 4. Owing to the **E**-field squared nature of the signal, the decay is proportional to $\exp(-2t/T_{pop})$ and, therefore, corresponds to population decay

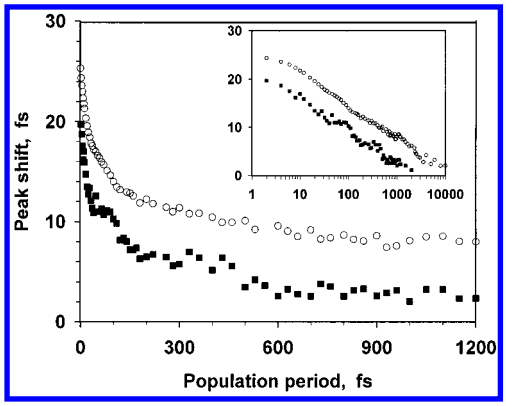

Figure 5. Experimental peak shift data for LHC-II. Filled squares are for Chl-*b* (650 nm) excitation, open circles for Chl-*a* (670 nm) excitation. The inset shows the same data for long time scales.

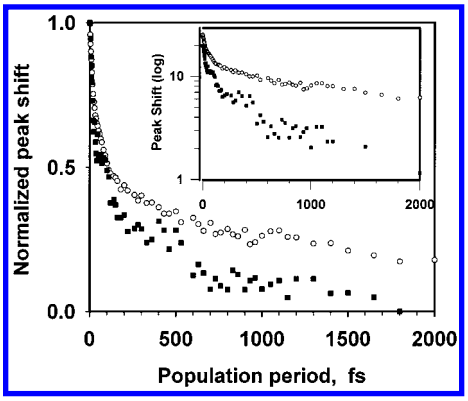

Figure 6. Normalized peak shift of Chl-*b* band (filled squares) and Chl-*a* band (open circles). (The asymptotic peak shift is subtracted from each data set prior to normalization.) Comparison of the normalized data sets clearly reveals faster decay components in Chl-*b* data. The inset shows the peak shift data (logarithmic scale) vs population time (linear scale) and it also reveals difference in the time scales of the decays of the peak shift data.

times of 320 fs and 4 ps. Because energy transfer within the laser spectrum (intraband) does not change the excited state population, it should not influence the TG decay. However, the TG data reported here does decay with time scales that reflect Chl-*a* to Chl-*a* energy transfer. A similar observation was reported for the core (LH1) and peripheral (LH2) antenna complexes of purple bacteria, i.e., the transient grating signal decayed with a time scale indicative of intraband energy transfer.[37] Transient grating can be sensitive to intraband energy transfer in two ways. First, note from Figure 3 that the 670 nm laser pulse does not completely span the Chl-*a* region of the absorption spectrum. Thus, energy transfer to pigments at the red edge of the Chl-*a* band does correspond to the removal of excited state population from the laser window. In addition, Fayer and co-workers, using the Green's function solution of the master equation, have shown that energy transfer to a dipole of random orientation leads to a decay of grating intensity.[47] Therefore, the TG experiment is sensitive to the depolarization of the population grating, which is induced by transfer of excitation from chromophore to chromophore within the laser window. The 320 fs decay observed in the transient grating signal at 670 nm is similar to the fastest Chl-*a* to Chl-*a* energy transfer times observed in pump−probe experiments[16,24] and is assigned to energy transfer within the Chls-*a*. The 4 ps decay observed in transient grating, which is also assigned to Chl-*a*-Chl-*a* energy transfer, probably reflects an average of the 3 and 6 ps components observed in the peak shift data (vide infra) and similar time scales observed in pump−probe experiments.[16,24]

The transient grating signal at 650 nm (Figure 4, solid squares) also decays biexponentially with time constants of 90 fs (∼75%) and 750 fs (∼15%) and therefore corresponds to population decay times of 180 fs and 1.5 ps. The 180 fs is similar to rapid Chl-*b* to Chl-*a* energy transfer observed in pump−probe and fluorescence upconversion experiments,[21−29] while the 1.5 ps component may represent an average of moderate (600 fs) and slower (∼5 ps) components also identified by other experiments.[21−29] The signal exhibits a slow or nondecaying component (∼10% amplitude) that may represent a subset of long-lived Chl-*b* as observed in transient absorption measurements.[14,24] In neither the 670 or 650 nm data could we detect any oscillatory features.

4B. **3PEPS Data at 670 nm**. The initial value of the 670 nm peak shift (shown in Figure 5, open circles) is ∼25 fs, which is comparable to the initial peak shift values reported previously for purple bacterial light-harvesting complexes[37] and the *Rb. sphaeroides* reaction center.[48] This large value is indicative of weak electron−phonon coupling in the protein environment. The peak shift decays to a value of ∼15 fs in 120 fs, then decays slowly over a range of time scales. The peak shift at 10 ps is ∼2 fs but it is difficult to see if the peak shift continues to decay for longer times owing to a marked deterioration in signal-to-noise ratio. The 670 nm peak shift data do not reveal any obvious oscillations.

4C. **3PEPS Data at 650 nm**. The absorption spectrum of LHC-II has a shoulder at ∼650 nm, which is attributed to Chl-*b* absorption (∼80%) and the vibronic band of Chl-*a* (∼20%); thus peak shift data (Figure 5, solid squares) obtained at 650 nm should represent primarily Chl-*b* dynamics (see further discussion below). An unusual dip is observed in the peak shift around 60 fs that we are not able to elucidate further at this stage. (The dip could not be simulated by including different vibrational modes in our $M(t)$.) The peak shift at 650 nm decays notably faster than the 670 nm peak shift. There is a concomitant decay in signal intensity, so we could collect the data only until 2.0 ps, where the peak shift appears to be nearly zero. The faster decay of the peak shift is shown clearly in the normalized and logarithmic comparisons of the two data sets in Figure 6. The oscillations observed in the peak are consistent with a 60 cm^{-1} mode and we believe this to be the first observation of coherent nuclear motion in the LHC-II pigment−protein complex.

4D. Simulation of the Peak Shift Data. The simulation of 3PEPS data for such a complex system is a formidable problem. It is necessary to disentangle the energy transfer dynamics from the electronic energy gap fluctuations described by $M(t)$, which we refer to as solvation dynamics. Equation 4 suggests a reasonable strategy provided the solvation dynamics can be described by a model consistent with earlier studies of bacteriochlorophyll−protein complexes not exhibiting energy transfer,[38] and similar data obtained for dilute chromophores in polymer glass samples.[39,49,50] In addition, eq 4 needs to be extended to multiexponential energy transfer kinetics, for example:

$$\tau^*(T) = \tau_0^*(T)\{a_1 \exp(-k_{EET1}T) + a_2 \exp(-k_{EET2}T) + a_3 \exp(-k_{EET3}T)\} \quad (7)$$

Note that this is only an approximate expression presented here for simplicity. For all simulations, we employed the exact expressions from the model of Yang and Fleming[40] which is appropriate for weakly coupled two-level chromophores, i.e., for incoherent excitation hopping. Accounting for the influence of excitonic interactions is thus precluded.

TABLE 1: Simulation Parameters for the $M(t)$ Used for 670 nm and 650 nm Peak Shift Data[a]

	coupling strength $\langle\Delta\omega^2\rangle^{1/2}$, cm^{-1}	τ, fs	υ, cm^{-1}	τ_{damping}, fs
Gaussian	125	50		
vibration	85		1146	100
vibration	85		986	100
vibration	60		746	100
inhomogeneity	175			

[a] The parameters for the solvation correlation function, or $M(t)$ in the absence of energy transfer, are given. The phases of all the vibrations are set to zero. For 670 nm data: Chl-*a* to Chl-*a* energy transfer (within the pulse spectrum) was modeled according to the amplitudes and energy transfer times: $A_1 = 40\%$, $\tau_1 = 350$ fs; $A_2 = 25\%$, $\tau_2 = 3$ ps; $A_3 = 35\%$, $\tau_3 = 6$ ps. For 650 nm data: Chl-*b* to Chl-*a* energy transfer (to outside of the pulse spectrum) was modeled using the following amplitudes and energy transfer times: $A_1 = 40\%$, $\tau_1 = 150$ fs; $A_2 = 40\%$, $\tau_2 = 600$ fs; $A_3 = 20\%$, $\tau_3 = 4$ ps. Chl-b_i to Chl-b_j energy transfer was modeled as a biexponential with time constants of 300 and 800 fs with equal amplitudes (see Figure 8a for the model used). To account for the oscillations in the 650 nm data we have added a damped cosine with a coupling strength, $\langle\Delta\omega^2\rangle^{1/2} = 40$ cm^{-1}, frequency, $\upsilon = 60$ cm^{-1}, and damping time, $\tau_{\text{damping}} = 1600$ fs.

The peak shift data obtained by Yu et al. on the B820 subunit of LH1—a system in which there is no energy transfer[38]—reveals that protein solvation dynamics is composed of an ultrafast solvation component followed by long time scale inhomogeneity. Similarly, peak shift data from polymer glasses doped with dilute chromophores have shown that the solvation dynamics in moderately disordered hosts consists of an ultrafast response and a long time inhomogeneity.[39,49,50] The diffusive processes in these systems are so slow that they can be regarded as static on the time scale of our experiments and thus correspond to inhomogeneous broadening.

Since we do not have any a priori information of the solvation dynamics of the LHC-II protein, our strategy is to initially model the bath $M(t)$ (i.e., $M(t)$ of a two-level system coupled only to a bath) with the B820 subunit peak shift parameters: a 60 fs Gaussian with 100 cm^{-1} coupling strength and an inhomogeneous width of 175 cm^{-1} (standard deviation, σ). We also included intramolecular vibrational frequencies of 1146, 986, and 746 cm^{-1}, which were obtained from high-resolution fluorescence spectroscopy and Raman spectra.[51,52] Thus, we begin with a reasonable description of the protein bath and vibrational dynamics in $M(t)$, which yields the $\tau_0^*(t)$ of eq 7. These parameters are adjusted slightly to improve comparison with the data, and energy transfer dynamics are included as described below.

Simulation of the 670 nm Peak Shift. To model the energy transfer kinetics, results reported by other workers[24,26,29] were incorporated into the model. In short, ~350 fs (~50% amplitude), ~3 ps (~25% amplitude), and ~6ps (25% amplitude) rate constants were used to simulate the decay in the peak shift data due to energy transfer. All the parameters were then adjusted slightly to give the best fit. We find that the peak shift is most sensitive to the time scale of the Gaussian component, its coupling strength, and the energy transfer parameters. The high-frequency vibrational modes improve the agreement of the peak shift in the first 100 fs, but are not well determined, as they are not sensitive fitting parameters.

The final parameters of the model $M(t)$ along with energy transfer rate constants and amplitudes that best simulate the peak shift data at 670 nm are given in Table 1, and the simulated peak shift is shown in Figure 7 as a solid line. The 50 fs Gaussian component is attributed to the rapid fluctuations of the protein environment and is predominantly responsible for the homogeneous broadening of the absorption spectrum. In general, proteins have been shown to mediate ultrafast solvation owing to the wide phonon band which spreads from 0 to 200 cm^{-1}.[53−58] Fluorescence studies at 4 K on LHC-II revealed a phonon sideband with a maximum at 80 cm^{-1} and followed by an exponential tail with a decay width of 200 cm^{-1}.[58,59] The Stokes shift, calculated by adding the reorganization energies of the Gaussian and low-frequency ($\hbar\omega < kT$) damped cosine components used for simulation of the 3PEPS data is ~100 cm^{-1}. As a consequence of the large initial peak shift, the coupling strengths used to simulate the LHC-II data are smaller than that characteristic of typical dilute chromophores dissolved in liquid solutions. This reflects the fact that the electron−phonon coupling in photosynthetic pigment−protein complexes in general is weak, promoting efficient energy transfer by limiting the dissipation of the excitation energy to the environment.

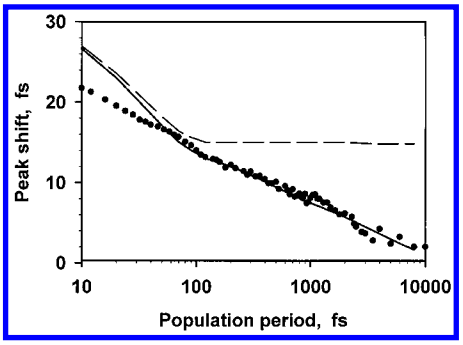

Figure 7. Simulated peak shift for 670 nm (Chl-*a*) using the parameters given in Table 1 (solid line). The dots represent the experimental peak shift data. Note the logarithmic scale for the population period. The dashed line is the peak shift for a noninteracting two-level system obtained via only the $M(t)$ given in Table 1 (i.e., no energy transfer).

The agreement between the experimental data and the simulation is not good for the first 60 fs due to at least two deficiencies: we do not include contributions from two-exciton states to the response function,[60,61] and the effect of energy transfer during the coherence periods is neglected. Either effect may lead to interfering echo terms which temporarily reduce the echo signal (increasing the ratio of FID to echo).[62] Thus, these factors may be responsible for a poor fitting of the peak shift in the first 60 fs.

Using only the $M(t)$ parameters, we calculated $\tau_0^*(T)$, i.e., the peak shift in the absence of energy transfer (shown as dashed line in Figure 7). Using the values of the rate constants and their respective amplitudes from our simulations, we then calculated $\tau^*(T)$ via eq 7. The $\tau^*(T)$ obtained by this procedure (data not shown) closely matches the peak shift obtained through the formal expressions for the response functions used in all our simulations. This illustrates that eq 7 is a useful expression for describing the peak shift of systems with (intraband) multiexponential energy transfer kinetics.

The Chl-*a* Q_y absorption band of LHC-II is believed to comprise absorption from a number (at least six) of spectral "types" of Chl-*a*.[18−20] The spectral equilibration among these Chls-*a* (that absorb within the laser window) is probed by the 3PEPS measurement. In agreement with previous work,[24,63] the peak shift data at 670 nm provides firm evidence that spectral equilibration among the Chls-*a* takes place over a wide range of time scales, which we approximate with time constants of 350 fs, 3ps, and 6 ps. Modeling the energy transfer kinetics by solving the master equation for the recently proposed structural

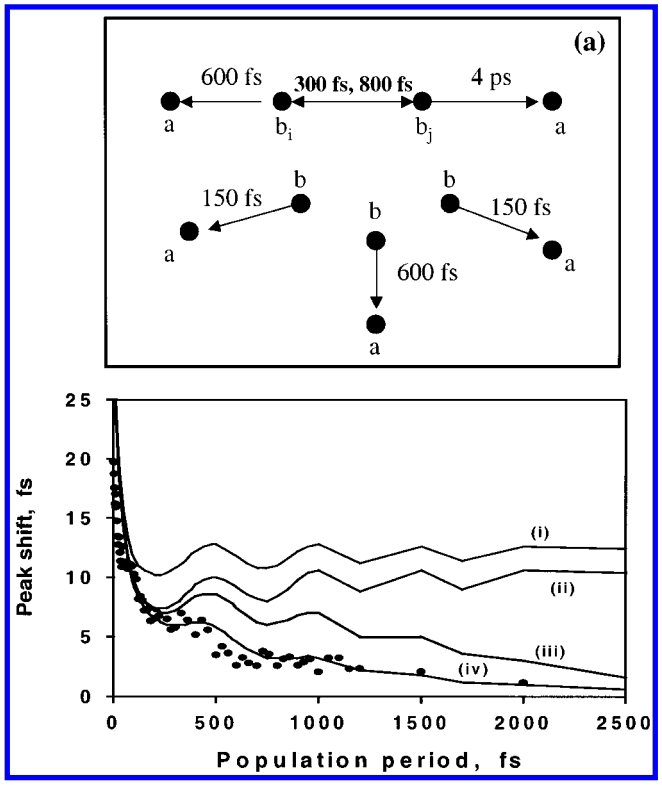

Figure 8. (a) A proposed model for energy transfer dynamics in LHC-II. The numbers indicate the energy transfer time scales. The double arrow between the intraband Chl-*b* pair is meant to indicate that either can act as a donor, not that we incorporate reversible energy transfer as described in section 4D. We model intra Chl-*b* pair dynamics with a biexponential kinetic scheme to mimics a reversible, disordered system. (b) Simulation of Chl-b data (see Table 1 for parameters) for different models: The experimental peak shift data are shown as dots. (i) Simulated peak shift for no Chl-*b* to Chl-*b* transfer (only Chl-*b* to Chl-*a* transfer). (ii) Simulation for the model given in part a but with Chl-b_i and Chl-b_j connected to Chls-*a* with an energy transfer time scales of 150 and 600 fs, respectively. The other Chl-*b* to Chl-*a* time scales are 150 fs, 600 fs, and 4 ps. The energy transfer time scales for Chl-b_i to Chl-b_j are as shown in part a. This model fails to simulate the experimental peak shift even for b_i to b_j energy transfer time set at 40 fs (100% amplitude). (iii) Simulation for the model given in part a but with Chl-b_i and Chl-b_j connected to Chls-*a* with an energy transfer time scales of 150 fs and 4 ps, respectively. The other Chl-*b* to Chl-*a* time scales are 150 and 600 fs ($\times 2$). The energy transfer time scales for Chl-b_i to Chl-b_j are as shown in part a. This model fails to simulate the experimental peak shift even for b_i to b_j energy transfer time set at 100 fs (100% amplitude). (iv) Simulated peak shift for the model given in part a.

assignments also reveals similar time scales of spectral equilibration between Chls-*a* molecules (discussed further in section 4E).

Simulation of the 650 nm Peak Shift. In order to simulate the 650 nm data (shown in Figure 8b), the bath $M(t)$ obtained from peak shift data at 670 nm was retained (i.e., we assume this provides a general representation of the coupling of the pigment to the protein environment). To account for the 60 cm^{-1} oscillation revealed by a simple fit to the peak shift data, a damped cosine was added to this $M(t)$ with a small coupling strength. Modeling of the energy transfer is more complex than for 670 nm excitation as we have to account for the energy transfer from Chl-*b* to Chl-*a*, i.e., transfer of excitation out of the laser spectrum. As discussed in section 3, energy transfer outside the laser spectrum (interband transfer) by itself does not lead to decay of the peak shift, but simply a reduction in signal intensity, since no signal (FID or echo) is generated by the acceptor. Why then, does the experimental peak shift at 650 nm decay to a near zero value in around 2 ps? While this may represent Chl-*b* to Chl-*b* (intraband) energy transfer, we must be aware of the possible presence of signal from Chls-*a*.

The peak shift could be affected by excited state absorption (ESA) of the Chl-*a* band at 650 nm. However, pump−probe data[24,27] and our transient grating data suggest that the excited state contribution comprises only 10%−15% of the total signal. Moreover, simulations including the effect of ESA of the acceptor chromophore did not give rise to decay of the peak shift; rather, ESA can lead to a slight increase of the peak shift.[64]

We must also consider overlap of the 650 nm pulse with blue "spectral types" of Chl-*a* (molecules in binding sites with shifted spectra).[19,20] Indeed, a Chl-*a* absorption at 661 nm has been suggested,[19,20] which would (weakly) overlap with the 650 nm excitation pulse (see Figure 3). If there is fast Chl-*b* to Chl-*a* (661 nm) energy transfer, then this would show up in the 3PEPS data as a fast exponential component. While this cannot be ruled out entirely, we note that previous studies[24,26,29] have suggested that Chl-*b* to Chl-*a* transfer populates only Chls-*a* absorbing around 675 and 680 nm, which lie well outside our pulse spectrum. A simple Förster rate calculation based on structural assignments proposed by Gradinaru et al.[16] and Trinkunas et al.[14] also did not reveal ultrafast energy transfer from any Chl-*b* (or Chl-*a*) to the Chls-*a* absorbing around 661 nm.

The most likely contribution of Chl-*a* signal to the 650 nm 3PEPS data arises from direct excitation of the vibronic band of Chl-*a*. Eads et al.[21] estimated the ratio of excitation of Chl-*b*:Chl-*a* at 650 nm to be approximately 5:1. Therefore, the contribution from the direct excitation of the vibronic band of Chl-*a* is expected to be ∼20% of the total signal. Simulating this signal is difficult as the effects of off-resonant (∼450 cm^{-1} in this case) excitation on the peak shift are poorly understood. Recent results from our laboratory on the B800 band of the peripheral LH2 complex of *Rps. acidophila*[65] suggest that peak shift data taken at wavelengths shifted toward the blue side of the absorption maximum show smaller initial peak shifts (population period = 0) than data taken at the absorption maximum. For a detuning of ∼300 cm^{-1} from the absorption maximum, the initial peak was observed to drop from ∼26 fs to ∼18 fs though the time scales of the of peak shift decay were not affected by detuning. Thus, if we were observing primarily Chl-*a* signal in the 650 nm data, the initial peak shift should be 14−16 fs (for a detuning of 450 cm^{-1}) and the long time decays should match the 670 nm data. As the 650 nm data have an initial peak shift of 20 fs and clearly decay faster (in the energy transfer regime) than the 670 nm data (see Figure 6), we suggest that the 650 nm peak shift data primarily reflect Chl-*b* dynamics.

To describe the 650 nm data, we incorporate both intra- (Chl-*b*−Chl-*b*) and inter-(Chl-*b*−Chl-*a*) band energy transfer into the model. Time-resolved studies of LHC-II have shown that energy transfer from Chl-*b* to Chl-*a* (interband) takes place on a wide range of time scales: 40% in less than 300 fs, 40% in ∼600 fs, and 20% in 4−9 ps.[14,22,24] A simulation with the above-mentioned Chl-*b* to Chl-*a* transfer rates but with no Chl-*b* to Chl-*b* energy transfer (shown in Figure 8, curve (i)) fails to reproduce the experimental data. Even adding a very fast Chl-*b* to Chl-*a* transfer rate (50 fs, 75% amplitude), which seems highly unlikely, could not reproduce the peak shift decay. This is not surprising as it was shown in section 3 that interband energy transfer alone has little effect on the peak shift. Therefore, we propose that the decay in the 650 nm peak shift is due to intraband (Chl-*b*−Chl-*b*) energy transfer dynamics. There has

been no previous direct experimental observation of intraband Chl-*b* dynamics in LHC-II to the best of our knowledge.

The most satisfactory method of modeling these data would be to combine a population kinetics of the excitation energy with a response function formalism as described in section 3. In this kind of approach, response functions associated with a population state contain information on the nuclear fluctuations determined by the initial state of the excitation energy and a proper nuclear time-evolution operator. Hence, in order to associate a proper response function with population kinetics, the history of the population evolution should be carefully described. In an irreversible energy transfer system, the nuclear fluctuation dynamics of all donor chromophores are equivalently described by a single statistical quantity (like $M(t)$). The population on an acceptor chromophore will see nuclear fluctuations uncorrelated with that of the donor and the theory we adopt incorporates this kind of behavior as mentioned in section 3. On the other hand, in a reversible energy transfer system (which may be the case for the present system with energy transfer between Chls-*b*), an excited chromophore which has existed continuously from the initial excitation and an excited chromophore which has been repopulated by a backward energy transfer process should be represented by different nuclear states. In this case, the response functions associated with the two donor chromophores with different histories should be distinct. We have no information about the population-history-dependent nuclear states of the donor; however, earlier work suggests that the nuclear fluctuations of the protein can be well characterized by short time scale fluctuations ($<$100 fs) and static (or very long time scale) components.[38] Based on this observation, we assume the energy transfer time scale ($>$300 fs) is longer than the dynamic component of the protein nuclear fluctuation. In this case, the response functions associated with the two types of donor chromophores will not depend on their history and will be identical for time scales longer than energy transfer time. These response functions for such time scales will retain only the static component of the nuclear line-shape function on the donor site. Within this approximation, regardless of the history of population transfer, the initial donor will produce equivalent characteristics of the signal (described by a response function) having the echo properties with respect to static disorder. Of course, while the excitation energy stays on the acceptor chromophore, the system will generate a FID signal that results in a decay of the peak shift. Then the formal structure of the total response function for reversible energy transfer system is identical to that for an irreversible energy transfer system. The only difference between the two cases is the difference in the population kinetics of the initial donor. In reversible energy transfer systems, the population kinetics associated with the initial donor should be the sum of population that has not experienced energy transfer and the population that returns to the donor due to backward transfer. This population (due to backward transfer) also does not lead to decay of peak shift. A decay of peak shift within our model arises due to net flow of population from the initial donor to the acceptor chromophore(s) (which generates the FID signal), while the details of the population transfer kinetics depend on the energy transfer mechanisms and energy transfer rates between the chromophore pairs. In the presence of static disorder, the kinetics of net energy flow should be obtained by an ensemble average over the disorder. This will lead to a complex multiexponential behavior of population kinetics. In this paper, this kind of complex kinetic behavior is approximated by simple biexponential kinetics (see Figure 8a). Of course, if there is no decay

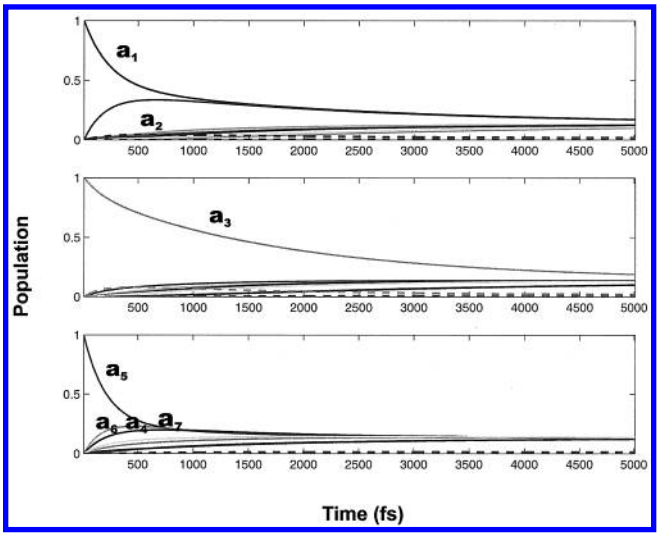

Figure 9. Population dynamics of LHC-II monomers for pigment assignment proposed by Gradinaru et al. The calculations place initial excitation on Chls-*a1*, -*a3*, and -*a5*, respectively, from top to bottom. The Chls-*a* population dynamics are shown by solid lines and Chls-*b* population dynamics by dashed lines.

channel of the excitation energy, an equilibration of energy between the Chls-*b* will occur so that the peak shift should not go to zero. However, in LHC-II, the excitation energy is rapidly transferred out of the laser window owing to energy transfer to Chls-*a* molecules and the present model of biexponential kinetics can approximately describe the kinetics of the preequilibrium phase between the Chls-*b*.

Let us restate that we are using biexponential, irreversible kinetics within the Chls-*b* to mimic the true, reversible kinetics of a disordered system. This approximation is valid because the energy transfer time scales are slower than the dynamic protein nuclear fluctuations.

The model we use for the 650 nm peak shift data (given in Figure 8a and simulated with curve (iv) in Figure 8b) is the following: a pair of Chls-*b* (b_i and b_j) are coupled to enable fast energy transfer between them, and these Chls-*b* are, in turn, connected to Chls-*a* by interband rates of $(600\ \text{fs})^{-1}$ and $(4\ \text{ps})^{-1}$, respectively. The intraband energy transfer kinetics (between Chls b_i and b_j) is given by a biexponential decay with time constants of 300 and 800 fs with equal amplitudes. The other three Chls-*b* are not coupled to each other but do transfer excitation to Chls-*a* with 150 fs (2 Chls-*b*) and 600 fs (1 Chl-*b*) time scales. Note that the interband time scales and amplitudes (2×150 fs, 2×600 fs, and 4 ps) are taken from earlier time-resolved data[14,22,24] (with the 2*x*, 2*x*, and 1*x* distribution also supported by master equation calculations, see section 4E and Figure 10a) and were not modified, as the simulation is quite insensitive to the interband parameters. In contrast, the decay of the simulated peak shift is sensitive to the time scales of intraband energy transfer (300 and 800 fs), that were determined via the fitting process.

The critical feature of this model is that slow Chl-*b*−Chl-*a* energy transfer is linked to the intraband Chl-*b* (b_i and b_j) pair. Chl-*b*−Chl-*a* energy transfer removes excited population from the laser window, so as the population period becomes larger, the peak shift becomes dominated by the Chls-*b* with the slowest Chl-*b* to Chl-*a* energy transfer rates. If these long-lived Chls-*b* did not participate in intraband energy transfer, then the 650 nm data would have decayed quite slowly. This is demonstrated by the solid line (ii) in Figure 8b—a simulation in which the intraband Chls-*b* are associated with more rapid Chl-*b* to Chl-*a*

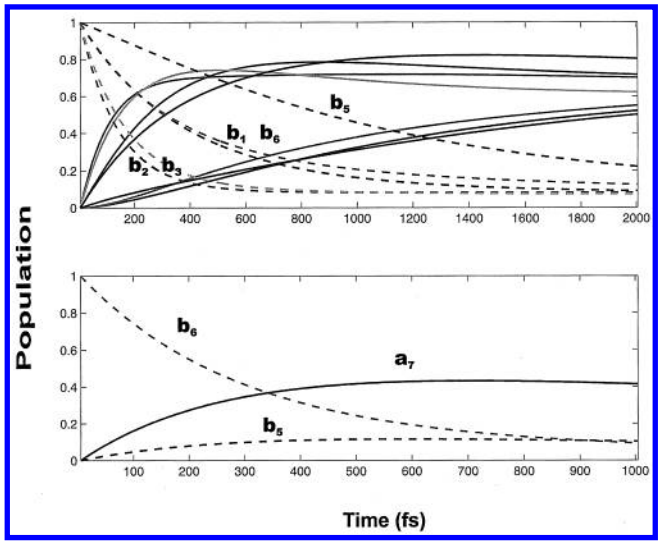

Figure 10. (a, top) Population dynamics of LHC-II monomers. The calculation is done by exciting all Chls-*b* with equal probabilities (dashed line) at $t = 0$ fs. The Chl-*a* population dynamics is shown by solid lines. (b, bottom) As in (a) but with initial population only on Chl-*b6*. Chl-*b* to Chl-*b* energy transfer is shown by the rise in Chl-*b5* population. Note that placing initial excitation on Chl-*a7* yields only a minor (∼2%) increase in Chl-*b5* population. Population dynamics of other Chls have been omitted for clarity.

energy transfer (150 and 600 fs) and the nonintraband Chls-*b* are connected with slower (150 fs, 600 fs, and 4 ps) Chl-*b*−Chl-*a* energy transfer. Using this model, we could not reproduce the experimental peak shift even with very fast (40 fs, 100% amplitude) Chl-*b* to Chl-*b* energy transfer. Also, a model with the Chl-*b* pair (b_i and b_j) coupled to Chls-*a* with transfer times of 150 fs and 4 ps could not simulate the experimental peak shift, as shown by the solid line (iii) in Figure 8b. Therefore, the decay of the 650 nm peak shift data to zero requires both rapid intraband energy transfer (which we assign to Chl-*b*−Chl-*b* transfer) and slow transfer of excitation away from both of those intraband energy transfer participants.

This analysis has assumed that each LHC-II complex exhibits the same structure and the same kinetic behavior. Recent results from Kuhlbrandt and co-workers[17] and Bassi et al.[18] suggest that several of the binding sites in LHC-II and the highly homologous CP-29 may bind either Chl-*b* or Chl-*a*. Thus, rather than some of the Chl-*b* from each complex engaging in intraband energy transfer, it may be that some fraction of the total number of complexes exhibits intraband Chl-*b* energy transfer, while others exhibit no Chl-*b*−Chl-*b* transfer.

As mentioned above, a 60 cm^{-1} vibrational mode was added to reproduce the slow modulations in the peak shift data. In a recent theoretical study by Renger et al., one- and two-color pump−probe spectra of LHC-II were simulated using the density matrix formalism.[66] The system was modeled as a collection of strongly coupled Chl *b*−Chl-*a* dimers, with each monomer being coupled to a 40 cm^{-1} vibrational mode, which in turn was coupled to the bath. Coherent oscillations were observed in one-color pump−probe simulated results at low temperatures. They also predicted coherent oscillations at higher temperatures if the damping parameter was lowered. The observation of the 60 cm^{-1} mode at room temperature in our data is rather surprising as it was not observed in a one-color pump−probe experiment.[26]

4E. Master Equation Calculations. Model calculations of energy transfer rates in LHC-II were undertaken for recently proposed assignments of various Chl-*b* and Chl-*a* sites within the structure to attempt to identify structural assignments that are consistent with the energy transfer rates identified from the peak shift data.

The energy transfer rates were estimated using Förster theory (i.e., incoherent hopping of excitation energy via transition dipole−transition dipole coupling).[67,68] For simplicity, all Chls-*a* (and Chls-*b*) were taken to be spectrally equivalent. The kinetics was determined by numerical solution of the coupled differential equations based on the Pauli master equation. The energetically "downhill" rate constants were calculated from the overlap of the donor emission spectrum and the acceptor absorption spectrum (cf. Förster equation). The uphill transfer rates were set according to detailed balance.[69] The dipole strengths were taken to be $\mu_a^2 = 24.65$ D^2 and $\mu_b^2 = 16.91$ D^2.[16] The absorption spectra were assumed to have Gaussian profiles with spectral widths $\sigma_a = 135$ cm^{-1} and $\sigma_b = 145$ cm^{-1} for Chl-*a* and Chl-*b*, respectively. The Stokes shift was taken to be 110 cm^{-1} for both Chl-*a* and Chl-*b*.[16] Calculations were carried out for two recently proposed assignments of pigment locations and orientations in LHC-II,[14,16] The discussion below centers on the structural assignments of Gradinaru et al.,[16] but the results mentioned here are qualitatively similar to the Trinkunas et al.[14] assignments as well. We follow the Kuhlbrandt (ref 8) site labeling convention and like to point out that Gradinaru et al. suggested that Chls-*a5* and -*b6* be swapped. Therefore, we use *a5* to refer to a Chl-*a* at a site labeled as *b6* by Kuhlbrandt and *b6* to a Chl-*b* at a site labeled as *a5*.

Because there remain unsettled questions regarding the specifics of Chl binding in LHC-II and because our model treats the pigment spectral types quite simply, we will refrain from discussing specific energy transfer rates and will confine our comments to general observations. Regarding Chl-*a*−Chl-*a* energy transfer, the most striking feature is the slow energy transfer from Chl-*a3* to all other Chl-*a*. Figure 9 shows the different dynamics for population placed initially in Chl-*a1*, -*a3*, and -*a5*. From the Chl-*a1* and -*a5* plots, it is clear that all of the Chl-*a* other than Chl-*a3* rapidly transfer energy to at least one other Chl-*a* (e.g., transfer between *a1* and *a2*, and transfer between *a4*, *a5*, *a6*, and *a7*).

Placing equal initial excitation on all Chls-*b* (Figure 10a) shows the transfer of energy from the Chls-*b* to the Chls-*a*. There are three distinct sets of Chl-*b* decay times, consistent with the model applied to the 650 nm peak shift data, and two sets of Chl-*a* rise times. Note that Chl-*b5* exhibits the longest lifetime and Chl-*b6* one of the intermediate lifetimes. Placing initial excitation on each of the Chls-*b* in turn reveals Chl-*b* to Chl-*b* energy transfer between Chl-*b5* and Chl-*b6*. Figure 10b shows the population dynamics after placing initial excitation on site Chl-*b6*. Population is quickly transferred to Chl-*a7*, but also to Chl-*b5*. Note that placing initial excitation on Chl-*a7* reveals only a small (∼2%) rise in Chl-*b5* population (data not shown), indicating that the rise in Chl-*b5* is really due to transfer from Chl-*b6*, though the pairwise rate we obtain (1300 fs) is substantially slower than that obtained from peak shift simulation.

Thus, master equation calculations (on *both* the Gradinaru et al. and Trinkunas et al. structural models) reveal energy transfer between a pair of Chls-*b* (*b5* and *b6* of Gradinaru et al.) along with slow transfer from those Chls-*b* to Chl-*a*, which is in qualitative agreement with the model proposed for the 650 nm peak shift data.

5. Conclusions

We have reported here the first three-pulse photon echo peak shift (3PEPS) measurements on the light harvesting complex

II (LHC-II) of a green algae *Chlamydomonas reinhardtii*. The results are analyzed using a new theory developed by Yang and Fleming[40] which formally incorporates the effect of energy transfer between weakly coupled donor−acceptor pairs on peak shifts. This analysis confirms the sensitivity of 3PEPS measurements to energy transfer between (approximately) isoenergetic chromophores, which is poorly addressed by conventional time-resolved techniques.

The peak shift data at 670 nm (Chl-*a* excitation) displays energy transfer time constants of 350 fs, 3 ps, and 6 ps which reflect the time scales of spectral equilibration within the Chls-*a*. Simulation of the peak shift data show that the electron−phonon coupling in the LHC-II complex is weak and the protein solvation can be modeled with a rapid (50 fs) Gaussian component (and intramolecular vibrations) followed by a long time inhomogeneity (static disorder).

Peak shift data obtained for Chl-*b* (650 nm) decays to a near zero value within 2 ps. Modulations in the peak shift data are modeled as a 60 cm^{-1} vibrational mode and attributed to coherent nuclear oscillations in LHC-II. Chl-*b* to Chl-*a* (interband) energy transfer cannot, by itself, lead to the observed decay in the peak shift. Thus, the 650 nm peak shift data strongly suggest excitation hopping within Chls-*b* (possibly between a pair of Chls-*b*) which transfer energy to Chls-*a* relatively slowly. The data are successfully simulated by a pair of Chls-*b* which transfer energy with 300 and 800 fs time constants and which transfer energy to Chls-*a* with 600fs and 4 ps time constants, while the remaining Chls-*b* transfer energy only to Chl-*a* with 150 and 600 fs time constants. Despite significant differences in the two recent structural assignments,[14,16] master equation calculations based on *both* assignments are in qualitative agreement with the model obtained by the peak shift simulation of the Chl-*b* band.

Note Added in Proof. Calculations and experimental studies of various solvated laser dyes recently undertaken in our laboratory have led us to believe that 3PEPS data are, in many cases, more sensitive to excitation wavelength than we previously thought. The results suggest that excitation centered on the blue edge of the absorption spectrum generally produces a lower initial peak shift value and a different temporal decay profile compared to those values obtained upon excitation at the red side of the absorption maximum. Although the 650 nm laser pulse in the LHC-II experiments reported here predominantly excites Chls-*b*, we are presently trying to incorporate properly the blue-edge Chl-*a* contribution to this signal into the 3PEPS simulations.

Acknowledgment. This work was supported by a grant from the NSF and in part by the donors of the Petroleum Research Fund of the American Chemical Society. M.Y. acknowledges the financial support of the Korea Research Foundation made in the program year 1997.

References and Notes

(1) Clayton, R. K. *Photosynthesis: Physical Mechanisms and Chemical Patterns*; Cambridge University Press: New York, 1980.

(2) van Grondelle, R.; Dekker, J. P.; Gillbro, T.; Sundström, V. *Biochim. Biophys. Acta* **1994**, *1187*, 1.

(3) Sundström, V.; Pullerits, T.; van Grondelle, R. *J. Phys. Chem. B* **1999**, *103*, 2327.

(4) Jansson, S. *Biochim. Biophys. Acta* **1994**, *1184*, 1.

(5) Green, B. R.; Durnford, D. G. *Annu. Rev. Plant Physiol. Plant Mol. Biol.* **1996**, *47*, 685.

(6) Bassi, R.; Giuffra, E.; Croce, R.; Dainese, P.; Bergantino, E. In *Light as an Energy Source and Informational Carrier in Plant Physiology*; Plenum Press: New York, 1996.

(7) Jennings, R. C.; Bassi, R.; Zucchelli, G. *Top. Curr. Chem.* **1996**, *177*, 147.

(8) Kühlbrandt, W.; Wang, D. N. *Nature* **1991**, *350*, 130.

(9) Kühlbrandt, W.; Wang, D. N.; Fujiyoshi, Y. *Nature* **1994**, *367*, 614.

(10) Peterman, E. J. G.; Gradinaru, C. C.; Calkoen, F.; Borst, J. C.; van Grondelle R.; *Biochemistry* **1997**, *36*, 12208.

(11) Hu, X.; Damjanovic, A.; Ritz, T.; Schulten, K. *Proc. Natl. Acad. Sci. U.S.A.* **1998**, *95*, 5935.

(12) Pullerits, T.; Sundström, V. *Acc. Chem. Res.* **1996**, *29*, 381.

(13) Krueger, B. P.; Scholes, G. D.; Yu, J.-Y.; Fleming, G. R. *Acta Phys. Pol. A* **1999**, *95*, 63.

(14) Trinkunas, G.; Connelly, J. P.; Müller, M. G.; Valkunas, L.; Holzwarth, A. R. *J. Phys. Chem. B* **1997**, *101*, 7313.

(15) Gülen, D.; van Grondelle, R.; van Amerongen, H. *J. Phys. Chem. B* **1997**, *101*, 7256.

(16) Gradinaru, C., C.; Ozdemir, S.; Gulen, D.; van Stokkum, I.; van Grondelle, R.; van Amerongen, H. *Biophys. J.* **1998**, *75*, 3064.

(17) Rogl, H.; Kuhlbrandt, W. *Biochemistry* **1999**, *38*, 16214.

(18) Bassi, R.; Croce, R.; Cugini, D.; Sandonna, D. *Proc. Natl. Acad. Sci. U.S.A.* **1999**, *96*, 10056.

(19) Hemelrijk, P. W.; Kwa, S. L. S.; van Grondelle, R.; Dekker: J. P. *Biochim. Biophys. Acta* **1992**, *1098*, 159.

(20) Nussberger, S.; Dekker, J. P.; Kuhlbrandt, W.; van Bolhuis, B. M.; van Grondelle, R.; van Amerongen, H. *Biochemistry* **1994**, *33*, 14775.

(21) Eads, D. D.; Castner, E. W.; Alberte, R. S.; Mets, L.; Fleming, G. R. *J. Phys. Chem.* **1989**, *93*, 8271.

(22) Du, M.; Xie, X.; Mets, L.; Fleming, G. R. *J. Phys. Chem.* **1994**, *98*, 4736.

(23) Pålsson, L. O.; Spangfort, M. D.; Gulbinas, V.; Gillbro, T. *FEBS Lett.* **1994**, *339*, 134.

(24) Visser, H. M.; Kleima, F. J.; van Stokkum, I. H. M.; van Grondelle, R.; van Amerongen, H. *Chem. Phys.* **1996**, *210*, 297.

(25) Kwa, S. L. S.; van Amerongen, H.; Lin, S.; Dekker, J. P.; van Grondelle, R.; Struve, W. S. *Biochim. Biophys. Acta* **1992**, *1102*, 202.

(26) Bittner, T.; Irrgang, K.-D.; Renger, G.; Wasielewski, M. R. *J. Phys. Chem.* **1994**, *98*, 11821.

(27) Bittner, T.; Wiederrecht, G. P.; Irrgang, K.-D.; Renger, G.; Wasielewski, M. R. *Chem. Phys.* **1995**, *194*, 311.

(28) Mullineaux, C. W.; Pascal, A. A.; Horton, P.; Holzwarth, A. R. *Biochim. Biophys. Acta* **1993**, *1141*, 23.

(29) Connelly, J. P.; Müller, M. G.; Hucke, M.; Gatzen, G.; Mullineaux, C. W.; Ruban, A. V.; Horton, P.; Holzwarth, A. R. *J. Phys. Chem. B* **1997**, *101*, 1902.

(30) Scholes, G. D.; Gould, I. R.; Cogdell, R. J.; Fleming, G. R. *J. Phys. Chem. B* **1999**, *103*, 2543.

(31) Krueger, B. P.; Scholes, G. D.; Fleming, G. R. *J. Phys. Chem. B* **1998**, *102*, 5378.

(32) Fiddler, H.; Knoester, J.; Wiersma, D. A. *J. Chem. Phys.* **1991**, *95*, 7880.

(33) Durrant, J. R.; Klug, D. R.; Kwa, S. L. S.; van Grondelle, R.; Porter, G.; Dekker, J. P. *Proc. Natl. Acad. Sci. U.S.A.* **1995**, *92*, 4798.

(34) Leegwater, J. A.; Durrant, J. R.; Klug, D. R. *J. Phys. Chem. B* **1997**, *101*, 7205.

(35) Fleming, G. R.; Cho, M. *Annu. Rev. Phys. Chem.* **1996**, *47*, 109.

(36) Yang, M.; Fleming, G. R. *J. Chem. Phys.* **1999**, *110*, 2983.

(37) Jimenez, R.; van Mourik, F.; Yu, J. Y.; Fleming, G. R. *J. Phys. Chem. B* **1997**, *101*, 7350.

(38) Yu, J.-Y.; Nagasawa, Y.; vanGrondelle, R.; Fleming, G. R. *Chem. Phys. Lett.* **1997**, *280*, 404.

(39) Nagasawa, Y.; Yu, J.-Y.; Cho, M.; Fleming, G. R. *Faraday Discuss.* **1997**, *108*, 23.

(40) Yang, M.; Fleming, G. R. *J. Chem. Phys.* **1999**, *111*, 27.

(41) Roitgrund, C. Ph.D. Thesis, The University of Chicago, 1989.

(42) Erickson, J. M.; Rahire, M.; Malnoe, P.; Girard-Bascou, J.; Pierre, Y.; Bennoun, P.; Rochiax, J.-D. *EMBO J.* **1999**, *5*, 1745.

(43) Bennoun, P.; Spierer-Herz, N.; Girard-Bascou, J.; Pierre, Y.; Delosme, M.; Rochaix, J.-D. *Plant Mol. Biol.* **1986**, *6*, 151.

(44) Joo, T.; Jia, Y.; Fleming, G. R. *J. Chem. Phys.* **1995**, *102*, 4063.

(45) Joo, T.; Jia, Y.; Yu, J.-Y.; Lang, M. J.; Fleming, G. R. *J. Chem. Phys.* **1996**, *104*, 1.

(46) Mukamel, S. *Principles of Nonlinear Optical Spectroscopy*; Oxford University Press: New York, 1995.

(47) Gochanour, C. R.; Anderson, H. C.; Fayer, M. D. *J. Chem. Phys.* **1979**, *70*, 4254.

(48) Groot, M.-L.; Yu, J.-Y.; Agarwal, R.; Norris, J. R.; Fleming, G. R. *J. Phys. Chem. B* **1998**, *102*, 5923.

(49) Nagasawa, Y.; Passino, S. A.; Joo, T.; Fleming, G. R. *J. Chem. Phys.* **1997**, *106*, 4840.

(50) Nagasawa, Y.; Yu, J.-Y.; Fleming, G. R. *J. Chem. Phys.* **1998**, *109*, 6175.

(51) Peterman, E. J. G.; Pullerits, T.; van Grondelle, R.; van Amerongen, H. *J. Phys. Chem. B* **1997**, *101*, 4448.

(52) Diers, J. R.; Zhu, Y.; Blankenship, R. E.; Bocian, D. F. *J. Phys. Chem.* **1996**, *100*, 8573.
(53) Brooks, C. L.; Karplus, M.; Pettitt, B. M. *Proteins: A Theoretical Perspective of Dynamics, Structure, and Thermodynamics*; J. Wiley: New York, 1988.
(54) Brooks, C. L.; Karplus, M. *J. Mol. Biol.* **1989**, *208*, 159.
(55) Ataka, M.; Tanaka, S. *Biopolymers* **1979**, *18*, 507.
(56) Gehlen, J. N.; Marchi, M.; Chandler, D. *Science* **1994**, *263*, 499.
(57) Schulten, K.; Tesch, M. *Chem. Phys.* **1991**, *158*, 421.
(58) Kuhn, O.; Renger, T.; Voigt, J.; Sundstrom, V. *Trends Photochem Photobiol.* **1997**, *4*, 213.
(59) Voigt, J.; Renger, T.; Schodel, R.; Schrotter, T.; Pieper, J.; Redlin, H. *Phys. Status Solidi* **1996**, *194*, 333.
(60) Renger, T.; May, V. *J. Phys. Chem. B* **1997**, *101*, 7232.
(61) Renger, T.; May, V. *Phys. Rev. Lett.* **1997**, *78*, 3406.
(62) Zhang, W. M.; Meier, T.; Chernyak, V.; Mukamel, S. *J. Chem. Phys.* **1998**, *108*, 7763.
(63) Gradinaru, C. C.; Pascal, A. A.; van Mourik, F.; Robert, B.; Horton, P.; van Grondelle, R.; van Amerongen, H. *Biochemistry* **1998**, *37*, 1143.
(64) Yang, M., unpublished results.
(65) Agarwal, R.; Fleming, G. R., manuscript in preparation.
(66) Renger, T.; Voigt, J.; May, V. *J. Phys. Chem.* **1996**, *100*, 15654.
(67) Förster, T. *Ann. Phys* **1948**, *2*, 55.
(68) Förster, T. In *Modern Quantum Chemistry*; Sinanoglu, O., Ed.; Academic Press: New York, 1965; Vol. III, p 93.
(69) Jean, J. M.; Chan, C.-K.; Fleming, G. R. *Isr. J. Chem.* **1988**, *28*, 169.